Cancer Research

Coactivation of AKT and β-Catenin in Mice Rapidly Induces Formation of Lipogenic Liver Tumors

Jimmy K. Stauffer[1], Anthony J. Scarzello[1], Jesper B. Andersen[2], Rachel L. De Kluyver[1], Timothy C. Back[1], Jonathan M. Weiss[1], Snorri S. Thorgeirsson[2], and Robert H. Wiltrout[1]

Abstract

Obesity is a risk factor for development of certain cancers but the basis for this risk is unclear. In this study, we developed a novel mouse model that demonstrates directly how lipogenic phenotypes commonly associated with diet-induced metabolic syndromes can influence hepatic cancer development. Activated AKT and β-catenin (*AKT*/*CAT*) genes were hydrodynamically codelivered using the Sleeping Beauty transposon to initiate liver tumorigenesis. AKT/CAT and MET/CAT combination induced microscopic tumor foci by 4 weeks, whereas no tumorigenesis resulted from delivery of AKT, MET, or CAT alone. Primary AKT/CAT tumor cells were steatotic (fatty) hepatocellular adenomas which progressed to hepatocellular carcinomas (HCC) upon *in vivo* passage, whereas primary MET/CAT tumors emerged directly as frank HCC. Conversion of AKT/CAT tumor cells to frank HCC during passage was associated with induction of the human HCC marker α-fetoprotein and the stem cell marker CD133. Using hierarchical clustering and gene set enrichment analysis, we compared the primary murine AKT/CAT and MET/CAT tumors to a panel of 53 human HCCs and determined that these two mouse models could be stratified as distinct subtypes associated in humans with poor clinical prognosis. The chief molecular networks identified in primary and passaged AKT/CAT tumors were steatosis and lipid metabolic pathways, respectively. Our findings show how coactivation of the AKT and CAT pathways in hepatocytes can efficiently model development of a lipogenic tumor phenotype. Furthermore, we believe that our approach could speed the dissection of microenvironmental factors responsible for driving steatotic-neoplastic transformation to frank carcinoma, through genetic modification of existing immunodefined transgenic models. *Cancer Res; 71(7); 2718–27. ©2011 AACR.*

Introduction

Knowledge of the genetic lesions associated with hepatocellular carcinoma (HCC) development has exploded in recent years with the advent of genome scale analysis and functional genomics (1). MET, β-catenin (CAT), and AKT are among the oncoproteins and signaling pathways frequently dysregulated in HCC. In human cancers including HCC, oncogenic MET is a regulator of metastasis, angiogenesis, and vascular invasion. The *MET* gene signature in HCC is correlated with very poor prognosis (2). Mutations in *CAT* occur in up to 50% of all HCCs. Many HCCs also demonstrate the activation of AKT and it has been reported that both hepatitis B and C can activate PI3K/AKT signaling (3). It is well established that AKT plays a key role in tumorigenesis by stimulating cell proliferation and inhibiting apoptosis. Phospho-AKT is also correlated with early disease reoccurrence and poor prognosis (4). It has been shown in several mouse models that driving hepatic AKT through either constitutively activated *AKT* or *PTEN* knockout or *E2f1* overexpression, results in lipogenic hepatocytes and steatohepatitis (5–7).

Molecular and epidemiologic studies show chronic infection with hepatitis virus B and C or exposure to environmental toxins is strongly associated with approximately 70% of HCC development. The remaining 30% of HCC is correlated with metabolic stress resulting from dietary factors and obesity (8). A common link between these diversely initiated etiologic pathways is the dependence upon inflammation. The initial hepatic transcriptional response to metabolic stress is induction of inflammation-associated genes which are eventually replaced with lipogenic genes resulting in hepatosteatosis with a clear cell appearance (9). Chronic dietary exposure results in a sustained inflammatory response that is further exacerbated by the fatty liver microenvironment resulting in steatohepatitis. Furthermore, a transcriptional regulatory link between lipogenesis, inflammation, and transformation has

Authors' Affiliations: [1]Cancer and Inflammation Program, NCI-Frederick, Frederick; and [2]Laboratory of Experimental Carcinogenesis, National Cancer Institute, Bethesda, Maryland

Note: Supplementary data for this article are available at Cancer Research Online (http://cancerres.aacrjournals.org/).

Corresponding Author: Robert H. Wiltrout, LEI NCI-Center for Cancer Research, NCI-Frederick, Bldg 428, Room 48A, Frederick, MD 21702. Phone: 301-846-1584; Fax: 1-301-846-1673; E-mail: wiltrour@mail.nih.gov

doi: 10.1158/0008-5472.CAN-10-2705

been recently established demonstrating that genes involved in these 3 networks are functionally interdependent in mediating oncogenesis (10).

A better understanding of the pathologic ability of preneoplastic precursor cells to perceive inflammatory mediators as tumorigenic growth signals may allow us to discover new opportunities for inhibiting or treating inflammation-driven hepatic cancers. As an initial step in determining what collaborative microenvironmental/extracellular signals predispose hepatocytes to tumorigenesis, we have developed and characterized an AKT/CAT-driven hepatic tumor model that accurately portrays the lipogenic phenotype seen in some human liver cancers. This model can rapidly be applied to any strain, displays progression, and is serially transplantable into syngeneic immunocompetent or transgenically immunodefined hosts (11).

Materials and Methods

Vector construction

pT3-EF5-flox, pT3-EF5-hMET, and HSB2 were provided by Dr. Xin Chen (UCSF, San Francisco, CA). A Δ90Nβ-catenin (first 90 amino acids deleted) was PCR amplified from RCAS-βCATS37AHA (Addgene; ref. 12) using the following primers: 5′-CACCACAATGGCTCAGAGGGTACGAGCT-3′ and 5′-TTACAGGTCAGTATCAAACC-3′. The Myr-AKT insert was PCR amplified from RCAS-myrAKT (Addgene; ref. 13) using the following primers: 5′-CACCCTTATGGGGAGCAGCAAG-3′ and 5′-TCAGGCTGTGCCACTGGCTGA-3′. These PCR products where cloned into pENTR (Invitrogen) and subsequently transferred to pT3-EF5-flox using the manufacturers protocol to produce pT3CAT and pT3AKT (Supplementary Fig. S1).

Hydrodynamic injection and monitoring

Hydrodynamic delivery and monitoring were done using strains FVB/n and C57/BL6 as previously described (11, 14). All mice were handled, fed, and housed in accordance with an approved NCI-Frederick Institutional Animal Care and Use protocol.

Orthotopic tumor passage

Tumor cell suspensions were made by physical dissociation of liver tumor in HBSS followed by filtration though 100-μm sieves. Cells (3×10^5 cells/0.5 mL) were administered as previously described (15).

Tissue collection and histology

Tumor-bearing livers were removed and each subdivided identically (by lobe) for subsequent analysis. Distinction between carcinoma and adenoma is based on trabeculation, differentiation, cell plate, and invasion (16).

Quantitative PCR

RNA was prepared from flash frozen tissue using the RNA miniprep kit (Qiagen) and AllPrep DNA/RNA miniprep kit (Qiagen). Analysis was performed according to ABI's manufacturer's protocol using the following primer sets (ABI identifier): keratin 19 (Mm00492980_m1), keratin 7 (Mm00466676_m1), tumor-associated calcium signal transducer 1 (Mm00493214_m1), α fetoprotein (AFP; Mm00431715_m1), delta-like 1 homolog (*Drosophila*; Mm00494477_m1), prominin 1 (Mm00477115_m1), dickkopf homolog 1 (*Xenopus laevis*; Mm00438422_m1), BMP (bone morphogenetic protein), and activin membrane–bound inhibitor homolog (*X. laevis*; Mm03024088_g1), and apolipoprotein C-I (Mm01319370_g1). mRNA expression levels were normalized to endogenous β-actin and expressed relative to normal livers. Data were log transformed and analyzed by one-way ANOVA and Tukey's *post hoc* test to determine statistical significance as indicated.

Transposon replication assay

A total of 100 ng DNA was subjected to *Dpn*I (10 units) digestion overnight at 37°C. Quantitative PCR (QPCR) was performed using the Taqman kit (ABI) with the following primers designed to a *pT3* promoter region that harbors 2 *Dpn*I sites:

T3Pr3′In.200F 5′-TGGAATTTGCCCTTTTTGAG-3′

T3Pr3′Ot/In.200/228R 5′-TCTGCAGAATTCCACCACAC-3′

Immunohistochemistry

Formalin-fixed slides were subjected to hematoxylin and eosin (H&E), Masson trichrome, periodic acid Schiff (PAS), tunnel (APO), and immunohistochemical (IHC) staining. The indirect immunoperoxidase procedure using ABC reagent kit [3,3′ diaminobenzidine (DAB) as chromogen], Vector Laboratories was used and the slides were stained with antibodies including the following: rabbit anti-human AFP (DakoCytomation; 1:500 dilution), CD45 (BD Biosciences; 1:100 dilution), LFABP (liver FABP; Santa Cruz; 1:500 dilution), β-catenin (Abcam; 1:100 dilution), and Ki67 (Abcam; 1:500 dilution). Formalin-fixed tissues were also cryopreserved and used for oil red O staining.

Microarray

A total of 200 ng RNA was amplified and incubated for 16 hours at 37°C (Ambion). The efficiency of the *in vitro* transcription was quantified using a NanoDrop ND1000 (Thermo Scientific). Array hybridization, washing, Cy3-streptavidin labeling (Amersham Biosciences), and scanning was performed on an iSCAN using reagents and protocols supplied by the manufacturer (Illumina, Inc.). A total of 750 ng biotinylated cRNA was hybridized to mouseRef-8v3 beadchips for 18 hours at 58°C. Image analysis and data extraction were automated using iSCAN Control Software (Illumina, Inc.).

Statistical analysis

Data collection was performed using GenomeStudio (Illumina, Inc.). The detection score for genes was computed from the *z* value relative to that of negative controls. The technical error was estimated by iterative robust least squares fit and the data set normalized using quantile algorithm and background subtraction. FDR (false discovery rate)-adjusted *P* values were calculated using the Benjamini–Hochberg procedure. Normal liver samples injected with empty T3 transposon were used as reference. All data were $\log_2$-transformed and

significant differentially expressed genes between the surrounding liver and tumor were identified by Bootstrap-t ($P \leq 0.001$; 5,000 repetitions). Integration of human HCC and mouse data sets was performed by *z*-transformation. The probability of overall survival was estimated according to Kaplan–Meier and Mantel–Cox statistics (GraphPad Prism5.01). Hierarchical cluster analysis based on Euclidian distance was performed with Cluster 3 and results were visualized with TreeView v1.6. Analysis of network connectivity was completed using Ingenuity Pathway Analysis (IPA7.1). The significance of each network and the connectivity was estimated in IPA. Nonparametric gene set enrichment analysis (GSEA) was performed with the GSEA tool developed by the Broad Institute.

Results

AKT cooperates with β-catenin to induce hepatocellular adenoma

The Sleeping Beauty (SB) transposon hydrodynamic injection system was selected to deliver transforming oncogenes to hepatocytes *in vivo* (Supplementary Fig. S1). We hypothesized that the codelivery of activated AKT and CAT in the liver would drive both steatogenesis and tumorigenesis. We compared the combination of activated AKT and CAT to MET and CAT which had been previously shown to induce HCCs by this method (11). Survival studies using FVB/n mice with either AKT or MET combined with CAT resulted in a median perimoribund liver tumor burden of 132 and 91 days, respectively (Fig. 1). No pathology was observed in single oncogene groups, demonstrating that oncogene cooperation is required for tumorigenesis using these specific oncogenes. The gross characteristics of the resulting tumors were dependent upon the genes delivered (Fig. 2A–C). The tumors were multifocal with greater than 100 nodules per liver. MET/CAT tumor was composed of tissue resembling normal liver and showing areas of intratumoral hemorrhage and bile-filled vesicles (Fig. 2A). The AKT/CAT tumors were pale, likely due to lipid accumulation, with intratumoral hemorrhage (Fig. 2B). Tumors were induced in both C57/BL6 and FVB/n mice with similar kinetics and penetrance. Histopathology identified foci of hyperplasia/neohepatocyte atypia along with HCC composed of cells with comparatively smaller cytoplasmic to nuclear volumes relative to adjacent hepatocytes in MET/CAT liver samples (Fig. 2D; MET/CAT P-0). Histopathology of AKT/CAT liver tumor samples revealed the presence of foci composed of vacuolated cells with large cytoplasm to nuclear volumes consistent with hepatocellular adenoma (HCA) and hepatosteatosis (Fig. 2D; AKT/CAT P-0). Histochemical staining with oil red O and PAS confirmed these vacuoles consisted of lipid and not glycogen (Supplementary Fig. S2A and B). IHC staining for AFP, a common HCC marker, showed areas of reactive cells only in MET/CAT but not in vector control (pT3) or AKT/CAT-transfected liver (Fig. 2E and data not shown).

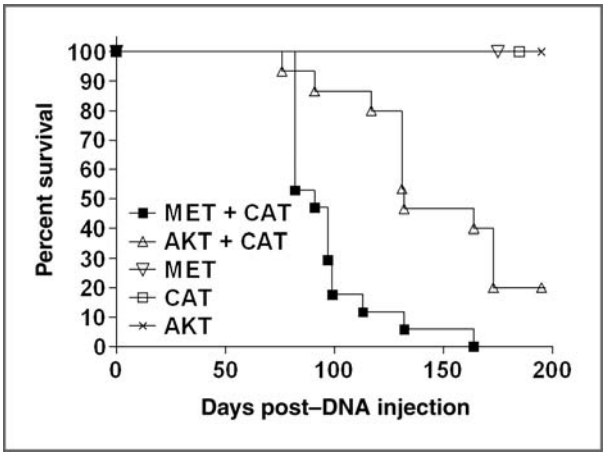

Figure 1. Survival after hydrodynamic delivery of oncogene expressing SB transposons. FVB/n mice (6–8 weeks) were administered 25 μg of the indicated oncogene by hydrodynamic tail vein injection. Mice were scored when perimoribund with tumor burden. MET/CAT: $n = 17$, AKT/CAT: $n = 15$, MET: $n = 5$, CAT: $n = 5$, and AKT: $n = 5$.

IHC stains characteristic of specific HCA subtypes and HCC-associated pathogenesis were also carried out on AKT/CAT and MET/CAT models (Fig. 3; ref. 17). Liver FABP loss, associated with the human HNF1 (hepatocyte nuclear factor 1-α)-deficient HCA subtype, did not occur in either AKT/CAT or MET/CAT models. Staining for β-catenin demonstrated tumor cell cytoplasmic and nuclear staining in both models. This is consistent with stabilized β-catenin transposition–dependent tumorigenesis and is a common feature of both HCC and the β-catenin subtype of HCA (17). An inflammation-associated increase in leukocyte infiltration was not evident by comparison of CD45-stained tumor and empty vector. However, staining for proliferation antigen Ki67 demonstrates the presence of morphologically smaller and elongated nuclei scattered throughout the tumor-bearing livers consistent with leukocyte proliferation and an inflammatory response in both tumor models. Tumor cell proliferation was more apparent in MET/CAT compared with AKT/CAT. Staining for apoptosis showed no evidence for model-associated cell death. Finally, Masson trichrome staining did not support the coinduction of fibrosis in these tumor models; however, isolated incidences of intratumoral connective tissue were evident in some higher passage AKT/CAT tumors (Supplementary Fig. S3 and data not shown).

Serial passage of AKT/CAT tumors correlates with increased malignancy

The ability to serially transplant tumors was tested by intrasplenic injection of 3×10^5 dispersed tumor cells. This approach assures hepatic dispersion of single cell suspension throughout the liver combined with pooling many primary tumors to further minimize the likelihood of clonal dominance or competition. Surprisingly, the MET/CAT tumors had a very long latency (Table 1), averaging 146 days compared with 91 days for the initial DNA driven tumor. Histology (Fig. 2D; MET/CAT P-1) shows little or no change in pathology. The second passage was carried out for more than 200 days

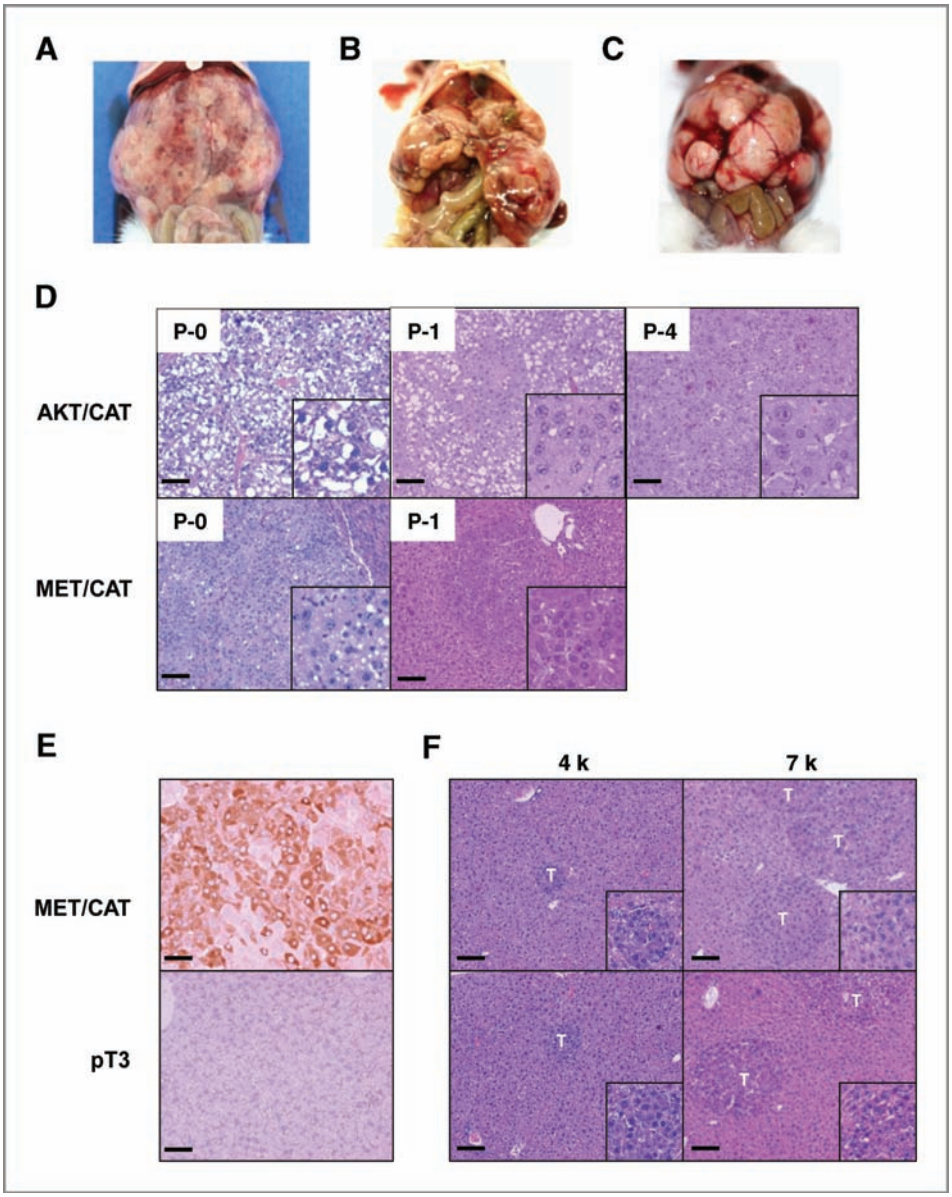

Figure 2. Gross morphology and histology of AKT/CAT and MET/CAT tumor models. A–C, hydrodynamic oncogene expressing SB tumors, (A) MET/CAT, (B) AKT/CAT, and (C) serially passaged AKT/CAT tumors. D, histology (H&E). 100×; bar, 100 μm; inset is 200× of AKT/CAT and MET/CAT tumors, top (P-0, P-1, P-4) are AKT/CAT tumor imaged at indicated passage progressing from clear cytoplasm (steatosis; HCA) to dense cytoplasm with trabeculation (HCC). Bottom, MET/CAT tumor (P-0, P-1) which does not show alteration upon passage. E, AFP immunohistochemistry (200×; bar, 50 μm). Seven-week MET/CAT and vector control (pT3)-transfected livers were stained for AFP protein. No staining was observed in vector control or in AKT/CAT transfected livers (data not shown). F, microscopic (100×; bar, 100 μm; inset is 200×) tumor growth in MET/CAT transfection can be detected as early as 4 weeks. T, tumor focus.

with no evidence of tumor. AKT/CAT tumor cells gave rise to perimoribund liver tumor masses (Fig. 2C) with latencies of 64 through 69 days for at least 4 serial passages (Table 1). Histochemical analysis showed that the degree of steatosis declined with passage resulting in denser cytoplasms, possible glycogen granules and accompanying trabeculation (Fig. 2D; AKT/CAT P-1, P-4). The incidence of invasiveness increased with passage reflected by the increase in proportion of carcinoma foci per passage (Table 1). This increase in carcinoma is consistent with a progressive transition from adenoma to carcinoma and supported by histology showing the dense cytoplasm phenotype within or attached to foci of clear cell appearance (Fig. 2D; AKT/CAT P-1, P-4). No evidence of extrahepatic metastatic or primary growth was detected using these hydrodynamically delivered oncogene combinations or by intrasplenic passage.

Expression patterns of hepatocyte and hepatic progenitor markers

To ascertain the relationship of these 2 tumor models to human HCC subtypes, a panel of human HCC prognostic signatures for hepatocyte and hepatic progenitor markers was employed (18). The MET/CAT model showed significant increases in hepatoblast markers AFP, DLK1, and CD133 relative to vector pT3 control–transfected liver (Fig. 4; $P < 0.05$). Primary AKT/CAT displayed no induction of AFP or CD133 and sporadic induction of DLK1. Upon passage, AKT/CAT tumors induced expression of AFP and CD133 to levels equal to the MET/CAT model with DLK1 remaining unchanged. Serial passages of AKT/CAT are stable with respect to AFP, CD133, KRT7, DKK1, BAMBI, and APOC1, whereas DLK1, Epcam, and KRT19 are highly variable consistent with clonal selection. Applying the human HCC

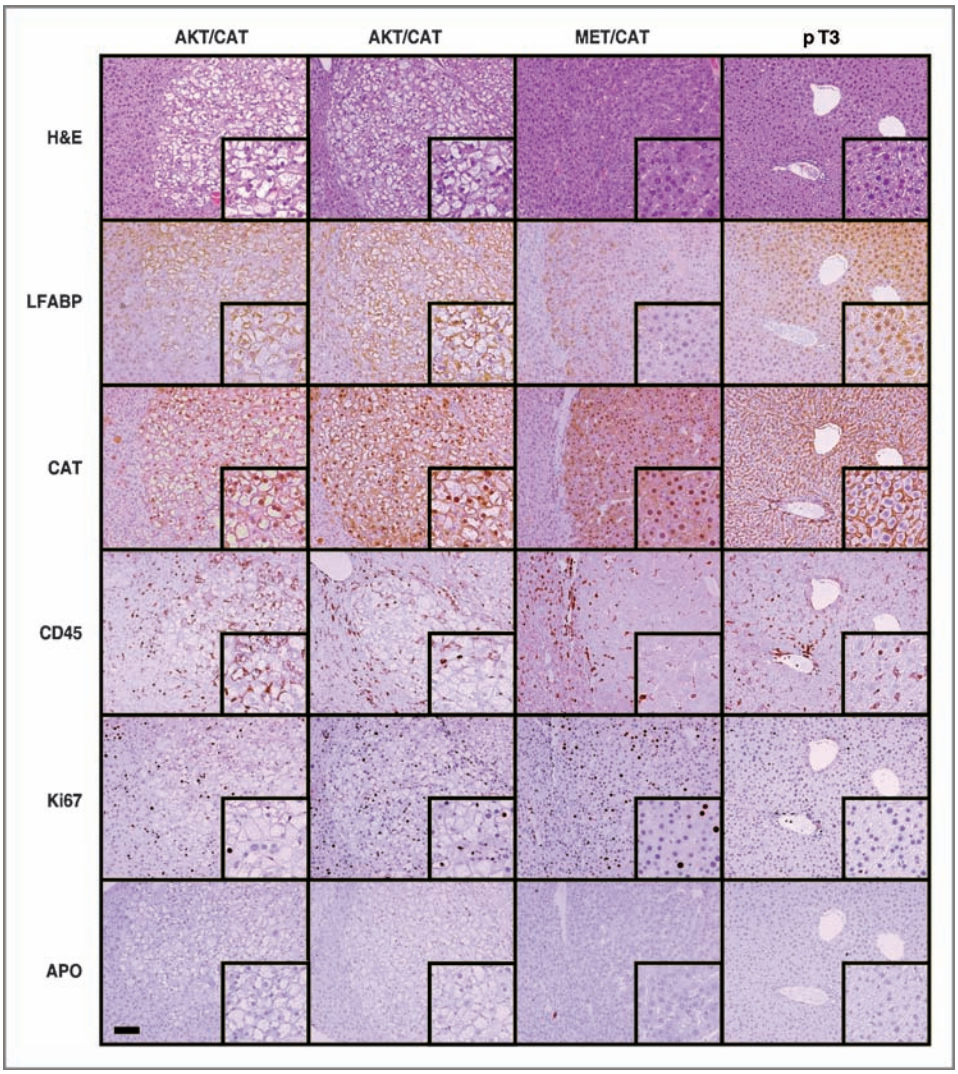

Figure 3. IHC analysis of HCA/HCC markers, apoptosis, leukocyte infiltration, and proliferation associated with AKT/CAT, MET/CAT, and control (pT3) liver. Stains are indicated in the left column and transposons are listed across the top. Two separate nodules from different livers were used for AKT/CAT. All slides are generated from serial sections (100×; bar, 100 μm; inset is 200×) and framed to show uninvolved liver tissue at the left margin for reference. LFABP staining was not altered in either model. β-Catenin staining (DAB) demonstrated tumor-specific nuclear accumulation in both models compared with adjacent liver tissue and control (pT3). CD45 staining shows little evidence of tumor infiltration; however, there is an increased incidence of CD45 staining in surrounding liver tissue. This coincides with Ki67 staining of small or elongated nuclei consistent with leukocyte proliferation. Ki67 staining indicates MET/CAT is proliferating more than AKT/CAT. There is no evidence of apoptosis in either model.

prognostic outcomes predicted by this panel as described previously (18), the resulting expression patterns stratify MET/CAT as a hepatocyte progenitor–like HCC (AFP^+, $Epcam^-$) with poor prognosis and primary AKT/CAT as mature hepatocyte-like HCC (AFP^-, $Epcam^-$) with fair prognosis. Upon serial passage of the AKT/CAT model, upregulation of AFP places it into the same hepatocyte progenitor–like/poor prognosis group as MET/CAT.

Development of an assay to selectively detect replication of integrated oncogene transposons as a sensitive surrogate marker of early tumorigenesis

To detect the earliest signs of tumor induction in this model, a trait or marker linked to the process of tumorigenesis was sought since histologic analysis indicated that liver tumors were difficult to observe prior to 4 weeks (Fig. 2F). We surmised that AFP is a likely candidate since it is a common marker of human HCC and it is upregulated several thousand-fold in end-stage MET/CAT tumors (Fig. 4). In addition, it has been shown by immunohistochemistry that AFP is not detectable in CAT- or MET-alone transfected livers but is robustly induced when these oncogenes are codelivered (11). By 3 days postinjection, AFP mRNA levels were not significantly different between MET/CAT and pT3 control vectors (Fig. 5A). An upward trend of 3-fold AFP message in oncogene DNA injected liver was evident at 1 week. At 2 weeks, AFP increased to a significant difference of 5-fold that was maintained through 4 weeks. Between 4 and 7 weeks, an average of 27-fold induction of AFP occurred.

Since different markers are unique to different collaborating oncogene pairs (no AFP in AKT/CAT; Fig. 4), a universal approach was developed that selectively quantitated, integrated, replicated transposon delivery vectors using *Dpn*I and QPCR. This assay measured the replication of transfected MET/CAT transposons in the same tumor samples used for AFP mRNA QPCR (Fig. 5B). The increase in transposon DNA occurred with similar kinetics to the increase in AFP message in the MET/CAT model. The replication assay shows a 2-fold greater sensitivity over AFP QPCR with respect to the empty vector control from

Table 1. Median time to perimoribund (days) and malignant composition as percentage carcinoma content from histologic classification (carcinoma/adenoma) upon serial passage of tumors generated by hydrodynamic transfection

	P-0	P-1	P-2	P-3	P-4
AKT/CAT					
Survival	132, $n = 15$	68, $n = 13$	67, $n = 51$	64, $n = 35$	69, $n = 11$
	range = 97	range = 154	range = 100	range = 117	range = 49
Malignancy	12.5%, $n = 4$	22.4%, $n = 12$	57.6%, $n = 38$	84.6%, $n = 25$	90.0%, $n = 10$
MET/CAT					
Survival	91, $n = 17$	146, $n = 6$	–	–	–
	range = 82	range = 93	–	–	–
Malignancy	25.4%, $n = 5$	58.3%, $n = 6$	–	–	–

3 days to 4 weeks although the first statistically significant difference matches with AFP QPCR at 14 days. Between 4 and 7 weeks, this difference increases from 10-fold to over 200-fold (relative to pT3 vector control) consistent with an increase in tumor growth but without a proportional increase in AFP message. Similar trends were observed with AKT/CAT (data not shown). Therefore, the replication assay is more sensitive than AFP QPCR and can be applied to any pT3 transposon–based model.

Comparative transcriptome analysis shows the AKT/CAT and MET/CAT relationship to human HCC

RNA was purified from a pool of 10 to 15 tumor nodules from each liver and subjected to expression analysis. This

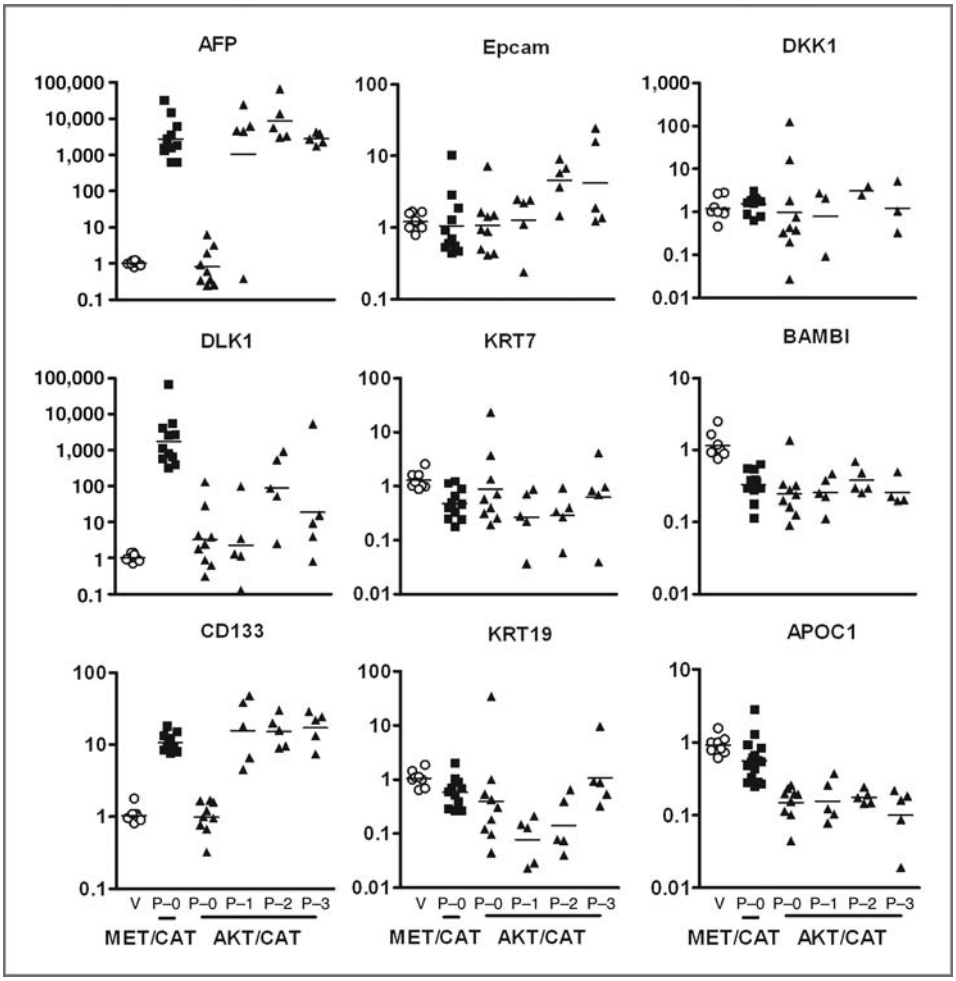

Figure 4. QPCR of HCC subtype associated and Epcam coregulated gene markers. The gene expression patterns generated by the following hepatic progenitor and differentiation markers can differentiate 4 subtypes of HCC (18). AFP, DLK1, and CD133 are stem/hepatoblast markers; Epcam, KRT7, and KRT19 are stem/epithelial markers; DKK1 and BAMBI are Wnt signaling markers; and APOC1 is a mature hepatocyte marker. Liver transfected with pT3 (empty vector: column V, open circle), MET/CAT P-0 tumors (column underscored: P-0, filled square) and AKT/CAT P-0 and serially passaged tumors (columns underscored: P-0 through P-3, filled triangle). Each symbol represents the QPCR signal normalized to β-actin and relative to the mean pT3 signal (set to 1) for the respective marker to generate fold induction. The bar designates the geometric mean value of each group.

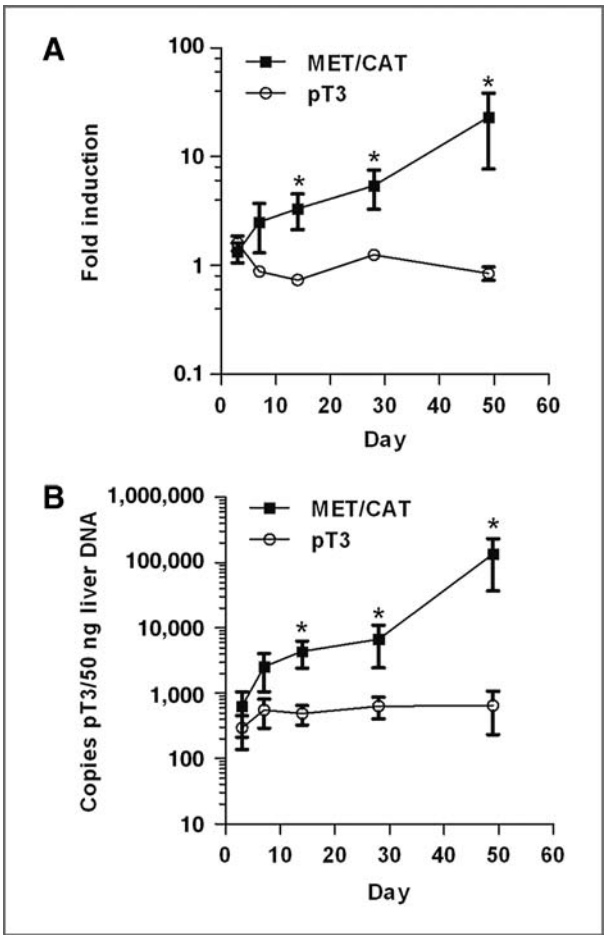

Figure 5. Detection of early tumorigenesis. A, QPCR for AFP message. This graph shows a 7-week time course of AFP mRNA expression in MET/CAT (10 μg, filled square) and vector control (pT3; 10 μg, open circle) transfected livers. *, statistically significant ($P < 0.05$) data points. days 3 and 7, $n = 5$; days 14, 28, and 49, $n = 10$. Symbols represent mean (SEM). B, transposon replication assay. Graph shows time course analysis of integrated transposon DNA replication (*Dpn*I digested, QPCR) for MET/CAT (10 μg, filled square) and vector control (pT3; 10 μg, open circle) transfected livers. *, statistically significant ($P < 0.05$) data points. days 3 and 7, $n = 5$; days 14, 28, and 49, $n = 10$.

included end point tumor harvested from initial MET/CAT ($n = 11$) and AKT/CAT ($n = 9$), and from serially passaged (P-3 and P-4; $n = 11$) AKT/CAT. Age-matched normal liver transfected with empty pT3 transposon vector ($n = 8$) was used as the control. Unsupervised hierarchical cluster analysis was carried out on a set of 1,953 genes that showed a differential expression (tumor to normal) of at least 2 in 50% of the samples and separated the tumors into 3 clusters according to the transfected DNA and passage (Fig. 6A). This confirmed that the modeling technique and the sampling method effectively squelched clonal variation and the resulting gene expression patterns were reproducible and specific to the transfected genes and not due to technical variability. Interestingly, AKT/CAT P-0 and MET/CAT P-0 are more similar than AKT/CAT P-0 is to passaged AKT/CAT (Fig. 6A). This may reflect the early stage of transformation in P-0 tumors likely dominated by a parental hepatic gene signature.

The association of the 2 tumor models and human HCC was further examined by cross-species comparison. The human HCC data set was generated from a cohort of 53 HCCs obtained from Caucasian and Chinese patients and hybridized to Illumina bead chips (19). Hierarchical cluster analysis (Supplementary Fig. S4) was performed on an integrated set of 53 human HCC and 11 MET/AKT P-0 (Fig. 6B) or 9 P-0 AKT/CAT (Fig. 6C)-derived murine tumors. A list of 2,403 or 833 orthologous genes between the 2 species (MET/CAT or AKT/CAT, respectively) represented on both platforms was identified. Integration and cluster analysis delineated clinically relevant subgroups of human HCC. Both the AKT/CAT- and MET/CAT-responsive gene signatures clustered predominantly with poor prognosis human HCCs according to the previous described A (poor prognosis) and B (good prognosis) subclassification (Fig. 6B and C; ref. 20). Cumulative survival analysis of the human HCC cases classified by MET/CAT and AKT/CAT gene signature clustering (Supplementary Fig. S5) verified this correlation ($P < 0.04$). GSEA of both the AKT/CAT and MET/CAT gene signatures demonstrated a significant positive correlation between upregulated genes and the gene expression signature of subclass A human HCC (Fig. 6D and E). Furthermore, GSEA of serial-passaged AKT/CAT tumors significantly increased the enrichment compared with AKT/CAT P-0 tumors, establishing a functional genomics correlation with serial passage and accompanying histologic changes (Figs. 6F and 2D).

Since the histology of AKT/CAT P-0 was characteristically clear cell indicating a high degree of cytoplasmic lipid, we hypothesized that this model may be reflecting the human phenotype driven largely by obesity through molecular mechanisms that depend on inflammatory mediators. IPA was used to identify statistically significant patterns of gene expression associated with known biological phenomena. Network comparison of AKT/CAT P-0 to MET/CAT P-0 gene expression revealed that liver steatosis is selectively associated with AKT/CAT P-0 ($P < 0.004$) and not MET/CAT P-0 ($P < 0.09$; Supplementary Fig. S6A). Steatohepatitis-associated genes were also selectively expressed in AKT/CAT P-0 but below the threshold of $P < 0.05$. Comparison of AKT/CAT primary to passaged tumor showed the most significant shared pathway in common was lipid metabolism ($P < 6.14 \times 10^{-6}$ and $P < 3.02 \times 10^{-11}$, respectively; Supplementary Fig. S6B). Ranking networks characterized as "molecular and cellular functions" ranked lipid metabolism as first and third of the 5 most significant pathways (Supplementary Table S1) in AKT/CAT P-3 and P-4 and AKT/CAT P-0, respectively. This corresponds to an increase of 94 to 218 proteins to this network, constituted in part by an induction of lipid catabolic genes (Supplementary Tables S2A and S2B) coinciding with the decrease in histologic steatosis (Fig. 2D) and increased malignancy. These transcriptome analyses are consistent with *AKT/CAT* gene expression resulting in hepatocytes acquiring a steatotic feature due to aberrant lipid metabolism that increases with malignancy (passaged AKT/CAT) accompanied by inflammation (steatohepatitis).

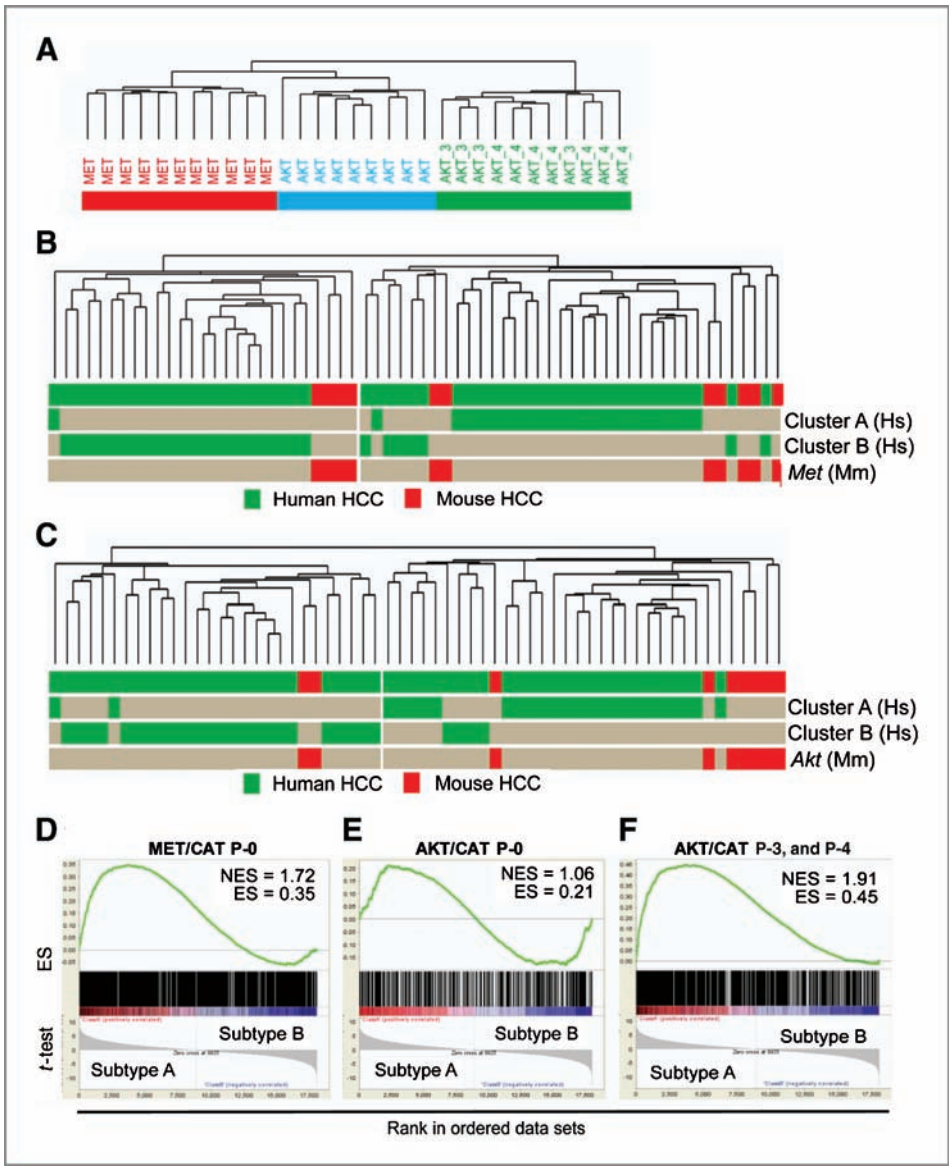

Figure 6. Comparative genomic analysis. A, hierarchical clustering of gene expression profiles from AKT/CAT P-0 (AKT), MET/CAT P-0 (MET), and serially passaged AKT/CAT (AKT-3, AKT-4) tumors. The relatedness of the respective transcriptional profiles is graphically represented by their arrangement in the dendrogram. B and C, dendrogram of unsupervised hierarchical cluster analysis of integrated human ($n = 53$), MET/CAT P-0 (B, $n = 11$) and AKT/CAT P-0 (C, $n = 9$) hepatocellular tumor transcriptomes (see Supplementary Fig. 4 for hierarchical clustering). The horizontal rows delineate the distribution of different cohorts and prognostic subclasses. The length of the branches is proportionate to the degree of transcriptome similarity. Differently shaded bars represent human and mouse HCC tissues (labeled at right end), respectively. To derive the AKT/CAT signature, tumor and surrounding liver tissue were utilized for analysis. The MET/CAT signature was derived by comparison with empty vector control liver since nontransformed tissue was not available. D–F, GSEA of gene signatures from MET/CAT P-0 (D), AKT/CAT P-0 (E), and passaged AKT/CAT P-3 and P-4 (F). Enrichment scores (ES) and normalized enrichment scores (NES) are shown. The *t* test is graphed below each correlated gene in the ranked data set. Passaging of AKT/CAT enriches (NES = 1.91) for human subtype A gene expression surpassing the association with MET/CAT signature (NES = 1.72).

Discussion

The combination of activated AKT and CAT rapidly produced steatotic liver tumors that favored adenoma pathology compared with carcinoma from MET and CAT (11). The AKT/CAT tumors were readily transplantable and became progressively malignant with increased passage in contrast to MET/CAT. This process was accompanied by an increase in cytoplasmic granularity and reduced lipid content. Microarray analysis confirmed that primary AKT/CAT tumors are steatogenic/lipogenic and that passage further expands the lipid metabolic network to include genes involved in lipid degradation and oxidation that could account for the concurrent reduction in lipid content.

The association of unique HCC tumor phenotypes with specific CAT activating mutations have been recently reported (21). Although conflicting accounts of β-catenin activation and prognostic outcomes exist, the activated β-catenin (deletion mutation) models described herein align with poor prognostic outcome (22–28). Integration and comparison with a human HCC cohort shows passaged AKT/CAT and MET/CAT models are associated with the poor prognosis subgroup (subtype A; ref. 20). Classification using a panel (18) of hepatocyte and hepatic progenitor markers derived from human HCC prognostic signatures stratify primary AKT/CAT tumor as mature hepatocyte-like HCC with fair prognosis contrasted to MET/CAT and serial-passaged AKT/CAT as hepatocyte progenitor–like HCCs with poor prognosis.

Although histopathology and molecular analysis classify primary AKT/CAT tumors as adenoma, AKT/CAT tumor growth more resembles MET/CAT carcinoma and is much more penetrant and aggressive than the previously reported MET/dominant-negative HNF1α adenoma model (11). This is consistent with the increased risk of malignant transformation observed in the activated β-catenin subtype of human HCA (17). Given that progression from adenoma to carcinoma is rarely observed during human HCC development and mouse AKT/CAT adenoma progresses to carcinoma, the transient mouse adenoma intermediate is likely a fortunate consequence perhaps reflecting a temporal extension in carcinoma development. The lack of an equivalent preneoplastic microenvironmental cue, such as fibrosis/cirrhosis, may contribute to this difference between mouse and human HCC development. Therefore, the primary AKT/CAT tumorigenesis model provides a useful bioassay for assaying host-mediated contributions to this malignant progression in the context of lipogenesis (hepatosteatosis).

The collaboration of the PI3K/AKT/mTOR and Wnt/β-catenin pathways in clear cell and HCC is supported by several lines of evidence. The PI3K/AKT/mTOR pathway is one of the most commonly utilized tumor signaling pathways able to stimulate proliferation, inhibit apoptosis, and drive anaerobic glycolysis (29, 30). Expression of constitutively activated AKT in liver has been shown to lead to excessive glucose utilization, lipogenesis, and hyperplasia but not malignancy (6). Liver-specific PTEN knockout results in AKT activation and produces very similar pathology including hepatomegaly, steatosis, and steatohepatitis (7). PTEN knockouts can progress to HCC at 66% to 83% penetrance but required 44 to 78 weeks and produce tumors that are very similar to human nonalcoholic steatohepatitis (NASH; ref. 31). The *CAT* gene is the most commonly mutated locus associated with HCC and adenoma that is predisposed to malignancy (32). Wnt/β-catenin signaling is activated in clear cell renal, endometrial, and ovarian cancers and can collaborate with the PTEN/AKT pathway in modeling mouse clear cell ovarian endometriod tumors (33, 34). Liver-specific expression of activated β-catenin produces hepatomegaly but not malignancy by itself. It has been shown to collaborate in hepatic tumorigenesis with MET, RAS, and Sprouty 2 utilizing the SB delivery system (35, 36). The resulting novel AKT/CAT model present here produces tumors more rapidly and with a higher penetrance than the existing transgenic models of HCC alone or in the context of hepatosteatosis (37).

Many lines of epidemiologic, clinical, and preclinical data are converging upon the linkage between obesity, inflammation, and oncogenesis. The liver is both an immunologic and metabolic interface where dietary antigens and metabolic byproducts are processed. The liver also displays the greatest sensitivity to obesity-linked cancer. The other types of cancers being linked to obesity include the clear cell subtypes of RCC (renal cell carcinoma) and ovarian cancer (38, 39). The molecular pathologic consequences of obesity in liver are steatosis and inflammation. Recently, the ability of obesity to promote tumorigenesis has been molecularly linked to pathways mediated by inflammatory cytokines (40). The steatotic liver tumor model presented here is applicable to existing transgenic immunodefined hosts, reproducible, rapid, displays malignant progression, and provides intrinsic molecular markers of early tumorigenesis. These attributes will accelerate our understanding of this linkage and perhaps suggests avenues of intervention into this form of liver cancer, as well as clear cell renal and epithelial-ovarian carcinomas.

Disclosure of Potential Conflicts of Interest

The content of this publication does not necessarily reflect the views or policies of the Department of Health and Human Services, nor does mention of trade names, commercial products, or organizations imply endorsement by the U.S. Government.

Acknowledgment

The authors thank Dr. John R. Ortaldo for assistance provided during the studies and suggestions made in the preparation of the manuscript.

Grant Support

This research was supported (in part) by the Intramural Research Program of the NIH, National Cancer Institute, Center for Cancer Research. This project has been funded in whole or in part with federal funds from the National Cancer Institute, NIH, under contract no. HHSN261200800001E.

The costs of publication of this article were defrayed in part by the payment of page charges. This article must therefore be hereby marked *advertisement* in accordance with 18 U.S.C. Section 1734 solely to indicate this fact.

Received July 23, 2010; revised January 22, 2011; accepted January 27, 2011; published OnlineFirst February 15, 2011.

References

1. Zender L, Villanueva A, Tovar V, Sia D, Chiang DY, Llovet JM. Cancer gene discovery in hepatocellular carcinoma. J Hepatol 2010; 52:921–9.
2. Kaposi-Novak P, Lee JS, Gomez-Quiroz L, Coulouarn C, Factor VM, Thorgeirsson SS. Met-regulated expression signature defines a subset of human hepatocellular carcinomas with poor prognosis and aggressive phenotype. J Clin Invest 2006;116: 1582–95.
3. Vinciguerra M, Foti M. PTEN at the crossroad of metabolic diseases and cancer in the liver. Ann Hepatol 2008;7:192–9.
4. Nakanishi K, Sakamoto M, Yamasaki S, Todo S, Hirohashi S. Akt phosphorylation is a risk factor for early disease recurrence and

poor prognosis in hepatocellular carcinoma. Cancer 2005;103: 307–12.
5. Coulouarn C, Gomez-Quiroz LE, Lee JS, Kaposi-Novak P, Conner EA, Goldina TA, et al. Oncogene-specific gene expression signatures at preneoplastic stage in mice define distinct mechanisms of hepatocarcinogenesis. Hepatology 2006;44:1003–11.
6. Ono H, Shimano H, Katagiri H, Yahagi N, Sakoda H, Onishi Y, et al. Hepatic Akt activation induces marked hypoglycemia, hepatomegaly, and hypertriglyceridemia with sterol regulatory element binding protein involvement. Diabetes 2003;52:2905–13.
7. Watanabe S, Horie Y, Suzuki A. Hepatocyte-specific Pten-deficient mice as a novel model for nonalcoholic steatohepatitis and hepatocellular carcinoma. Hepatol Res 2005;33:161–6.
8. Parekh S, Anania FA. Abnormal lipid and glucose metabolism in obesity: implications for nonalcoholic fatty liver disease. Gastroenterology 2007;132:2191–207.
9. Radonjic M, de Haan JR, van Erk MJ, van Dijk KW, van den Berg SA, de Groot PJ, et al. Genome-wide mRNA expression analysis of hepatic adaptation to high-fat diets reveals switch from an inflammatory to steatotic transcriptional program. PLoS One 2009;4:e6646.
10. Hirsch HA, Iliopoulos D, Joshi A, Zhang Y, Jaeger SA, Bulyk M, et al. A transcriptional signature and common gene networks link cancer with lipid metabolism and diverse human diseases. Cancer Cell 2010;17:348–61.
11. Tward AD, Jones KD, Yant S, Cheung ST, Fan ST, Chen X, et al. Distinct pathways of genomic progression to benign and malignant tumors of the liver. Proc Natl Acad Sci U S A 2007;104: 14771–6.
12. Orford K, Crockett C, Jensen JP, Weissman AM, Byers SW. Serine phosphorylation-regulated ubiquitination and degradation of beta-catenin. J Biol Chem 1997;272:24735–8.
13. Orsulic S, Li Y, Soslow RA, Vitale-Cross LA, Gutkind JS, Varmus HE. Induction of ovarian cancer by defined multiple genetic changes in a mouse model system. Cancer Cell 2002;1:53–62.
14. Patil MA, Lee SA, Macias E, Lam ET, Xu C, Jones KD, et al. Role of cyclin D1 as a mediator of c-Met- and beta-catenin-induced hepatocarcinogenesis. Cancer Res 2009;69:253–61.
15. Lee JK, Sayers TJ, Brooks AD, Back TC, Young HA, Komschlies KL, et al. IFN-gamma-dependent delay of *in vivo* tumor progression by Fas overexpression on murine renal cancer cells. J Immunol 2000;164:231–9.
16. International Classification of Rodent Tumors The Mouse. WHO International Agency for Research on Cancer. In:Mohr U, editor. New York: Springer-Verlag 2001; p. 64–8.
17. Bioulac-Sage P, Balabaud C, Zucman-Rossi J. Subtype classification of hepatocellular adenoma. Digestive surgery 2010;27:39–45.
18. Yamashita T, Forgues M, Wang W, Kim JW, Ye Q, Jia H, et al. EpCAM and alpha-fetoprotein expression defines novel prognostic subtypes of hepatocellular carcinoma. Cancer Res 2008;68:1451–61.
19. Andersen JB, Loi R, Perra A, Factor VM, Ledda-Columbano GM, Columbano A, et al. Progenitor-derived hepatocellular carcinoma model in the rat. Hepatology 2010;51:1401–9.
20. Lee JS, Chu IS, Heo J, Calvisi DF, Sun Z, Roskams T, et al. Classification and prediction of survival in hepatocellular carcinoma by gene expression profiling. Hepatology 2004;40:667–76.
21. Cieply B, Zeng G, Proverbs-Singh T, Geller DA, Monga SP. Unique phenotype of hepatocellular cancers with exon-3 mutations in beta-catenin gene. Hepatology 2009;49:821–31.
22. Hsu HC, Jeng YM, Mao TL, Chu JS, Lai PL, Peng SY. Beta-catenin mutations are associated with a subset of low-stage hepatocellular carcinoma negative for hepatitis B virus and with favorable prognosis. Am J Pathol 2000;157:763–70.
23. Wong CM, Fan ST, Ng IO. beta-Catenin mutation and overexpression in hepatocellular carcinoma: clinicopathologic and prognostic significance. Cancer 2001;92:136–45.
24. Fujito T, Sasaki Y, Iwao K, Miyoshi Y, Yamada T, Ohigashi H, et al. Prognostic significance of beta-catenin nuclear expression in hepatocellular carcinoma. Hepatogastroenterology 2004;51:921–4.
25. Yamaoka H, Ohtsu K, Sueda T, Yokoyama T, Hiyama E. Diagnostic and prognostic impact of beta-catenin alterations in pediatric liver tumors. Oncol Rep 2006;15:551–6.
26. Cavard C, Colnot S, Audard V, Benhamouche S, Finzi L, Torre C, et al. Wnt/beta-catenin pathway in hepatocellular carcinoma pathogenesis and liver physiology. Future Oncol 2008;4:647–60.
27. Yamashita T, Ji J, Budhu A, Forgues M, Yang W, Wang HY, et al. EpCAM-positive hepatocellular carcinoma cells are tumor-initiating cells with stem/progenitor cell features. Gastroenterology 2009; 136:1012–24.
28. Liu L, Zhu XD, Wang WQ, Shen Y, Qin Y, Ren ZG, et al. Activation of beta-catenin by hypoxia in hepatocellular carcinoma contributes to enhanced metastatic potential and poor prognosis. Clin Cancer Res 2010;16:2740–50.
29. Carnero A, Blanco-Aparicio C, Renner O, Link W, Leal JF. The PTEN/PI3K/AKT signalling pathway in cancer, therapeutic implications. Curr Cancer Drug Targets 2008;8:187–98.
30. Robey RB, Hay N. Is Akt the "Warburg kinase"?-Akt-energy metabolism interactions and oncogenesis. Semin Cancer Biol 2009;19:25–31.
31. Horie Y, Suzuki A, Kataoka E, Sasaki T, Hamada K, Sasaki J, et al. Hepatocyte-specific Pten deficiency results in steatohepatitis and hepatocellular carcinomas. J Clin Invest 2004;113:1774–83.
32. Imbeaud S, Ladeiro Y, Zucman-Rossi J. Identification of novel oncogenes and tumor suppressors in hepatocellular carcinoma. Semin Liver Dis 2010;30:75–86.
33. Zorn KK, Bonome T, Gangi L, Chandramouli GV, Awtrey CS, Gardner GJ, et al. Gene expression profiles of serous, endometrioid, and clear cell subtypes of ovarian and endometrial cancer. Clin Cancer Res 2005;11:6422–30.
34. Wu R, Hendrix-Lucas N, Kuick R, Zhai Y, Schwartz DR, Akyol A, et al. Mouse model of human ovarian endometrioid adenocarcinoma based on somatic defects in the Wnt/beta-catenin and PI3K/Pten signaling pathways. Cancer Cell 2007;11:321–33.
35. Wangensteen KJ, Wilber A, Keng VW, He Z, Matise I, Wangensteen L, et al. A facile method for somatic, lifelong manipulation of multiple genes in the mouse liver. Hepatology 2008;47:1714–24.
36. Lee SA, Ho C, Roy R, Kosinski C, Patil MA, Tward AD, et al. Integration of genomic analysis and *in vivo* transfection to identify sprouty 2 as a candidate tumor suppressor in liver cancer. Hepatology 2008;47: 1200–10.
37. Newell P, Villanueva A, Friedman SL, Koike K, Llovet JM. Experimental models of hepatocellular carcinoma. J Hepatol 2008;48: 858–79.
38. Lowrance WT, Thompson RH, Yee DS, Kaag M, Donat SM, Russo P. Obesity is associated with a higher risk of clear-cell renal cell carcinoma than with other histologies. BJU Int 2009;105:16–20.
39. Olsen CM, Nagle CM, Whiteman DC, Purdie DM, Green AC, Webb PM. Body size and risk of epithelial ovarian and related cancers: a population-based case-control study. Int J Cancer 2008;123:450–6.
40. Park EJ, Lee JH, Yu GY, He G, Ali SR, Holzer RG, et al. Dietary and genetic obesity promote liver inflammation and tumorigenesis by enhancing IL-6 and TNF expression. Cell 2010;140:197–208.